International Journal of Nanomedicine

Dovepress

open access to scientific and medical research

Open Access Full Text Article

ORIGINAL RESEARCH

Development of Ac2-26 Mesoporous Microparticle System as a Potential Therapeutic Agent for Inflammatory Bowel Diseases

Milena Fronza Broering[1,2], Pedro Leonidas Oseliero Filho[3,4], Pâmela Pacassa Borges[1], Luis Carlos Cides da Silva[3], Marcos Camargo Knirsch[5], Luana Filippi Xavier[1], Pablo Scharf[1], Silvana Sandri[1], Marco Antonio Stephano[5], Fernando Anselmo de Oliveira[6], Ibrahim M Sayed[2], Lionel Fernel Gamarra[6], Soumita Das[2], Márcia CA Fantini[3], Sandra HP Farsky[1]

[1]Department of Clinical and Toxicological Analyses, School of Pharmaceutical Sciences, University of São Paulo, São Paulo, SP, Brazil; [2]Department of Biomedical and Nutritional Sciences, University of Massachusetts, Lowell, MA, USA; [3]Department of Applied Physics, Physics Institute, University of Sao Paulo, São Paulo, Brazil; [4]Materials Innovation Factory, University of Liverpool, Liverpool, MSY, UK; [5]Department of Biochemical and Pharmaceutical Technology, School of Pharmaceutical Sciences, University of São Paulo, São Paulo, SP, Brazil; [6]Instituto do Cérebro, Instituto Israelita de Ensino e Pesquisa, Sociedade Beneficente Israelita Brasileira Hospital Albert Einstein, São Paulo, SP, Brazil

Correspondence: Sandra HP Farsky, Email sfarsky@usp.br

Introduction: Inflammatory bowel diseases (IBDs) disrupt the intestinal epithelium, leading to severe chronic inflammation. Current therapies cause adverse effects and are expensive, invasive, and ineffective for most patients. Annexin A1 (AnxA1) is a pivotal endogenous anti-inflammatory and tissue repair protein in IBD. Nanostructured compounds loading AnxA1 or its active N-terminal mimetic peptides improve IBD symptomatology.

Methods: To further explore their potential as a therapeutic candidate, the AnxA1 N-terminal mimetic peptide Ac2-26 was incorporated into SBA-15 ordered mesoporous silica and covered with EL30D-55 to deliver it by oral treatment into the inflamed gut.

Results: The systems SBA-Ac2-26 developed measurements revealed self-assembled rod-shaped particles, likely on the external surface of SBA-15, and 88% of peptide incorporation. SBA-15 carried the peptide Ac2-26 into cultured Raw 264.7 macrophages and Caco-2 epithelial cells. Moreover, oral administration of Eudragit-SBA-15-Ac2-26 (200 µg; once a day; for 4 days) reduced colitis clinical symptoms, inflammation, and improved epithelium recovery in mice under dextran-sodium sulfate-induced colitis.

Discussion: The absorption of SBA-15 in gut epithelial cells is typically low; however, the permeable inflamed barrier can enable microparticles to cross, being phagocyted by macrophages. These findings suggest that Ac2-26 is successfully delivered and binds to its receptors in both epithelial and immune cells, aligning with the clinical results.

Conclusion: Our findings demonstrate a simple and cost-effective approach to delivering Ac2-26 orally into the inflamed gut, highlighting its potential as non-invasive IBD therapy.

Keywords: annexin A1, SBA-15, oral route, tissue recovery, inflammation

Introduction

The incidence of IBDs has increased in the last decades in developed and newly industrialized countries. IBDs are relapsing and chronic inflammatory diseases which can affect the intestines and can be divided into two distinct types: ulcerative colitis (UC) and Crohn's disease (CD).[1] Both UC and CD patients present debilitating symptoms such as tenesmus, bloody stool, diarrhea, and fatigue.[2] Notably, malignant colorectal cancer, small bowel cancer, intestinal lymphoma, and cholangiocarcinoma are more common in IBD patients; in addition, the high incidence of neoplasms is related to IBD treatment, implicating the adverse effects of available drugs.[3] In addition to the considerable worsening situation that patients with IBD need to confront, approximately 50% of patients fail or experience a decrease in the effectiveness of available drugs. Furthermore, the most recent biological treatments are expensive and require invasive

Received: 24 November 2023
Accepted: 29 March 2024
Published: 12 April 2024

Graphical Abstract

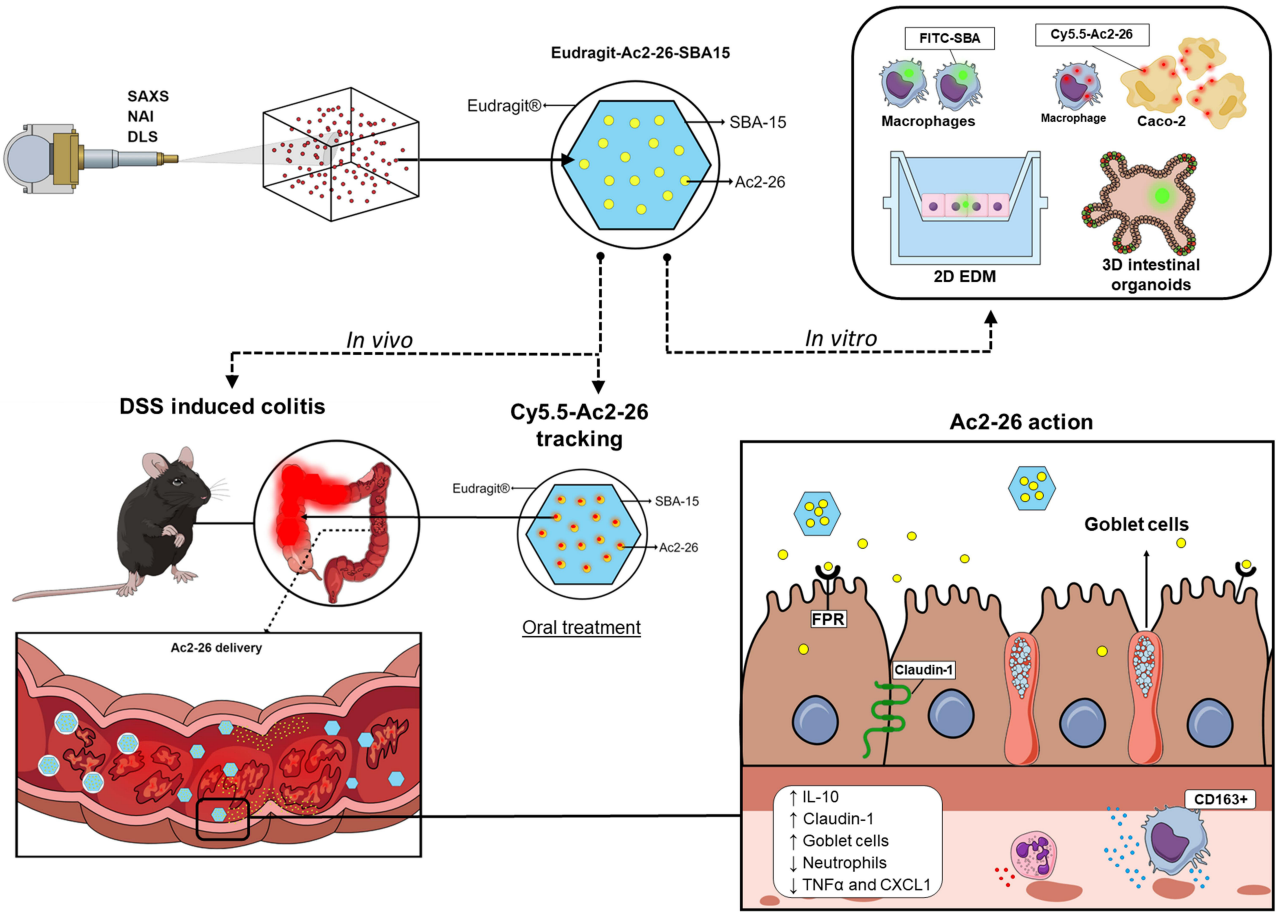

administration. These features make IBD a remarkable public health problem worldwide.[1,4] Hence, novel biological targets and drugs and pharmaceutical approaches for the delivery of noninvasive drug hallmarks of IBD are needed as subjects of biological and drug development research.[5]

AnxA1 is a 37 kDa endogenous protein and comprises the calcium and phospholipid-binding annexin superfamily.[6,7] Annexins present a C-terminal and an N-terminal domain specific for each superfamily component and confer specificity to biological activities.[7] AnxA1 was first characterized as a glucocorticoid-regulated anti-inflammatory protein;[6,8,9] currently, AnxA1 is recognized as a potent anti-inflammatory and resolving molecule that is a mediator of cell proliferation, differentiation, and immune, epithelial, and cancer cell apoptosis.[10–12] AnxA1 binds to intracellular structures, membrane phospholipids, or G-transmembrane-coupled formyl peptide receptors to trigger downstream activation of the intracellular pathway.[8]

Robust evidence has revealed the pivotal role of AnxA1 in the control of IBDs; as such, infiltrating leukocytes and epithelial intestinal cells express this protein during the course of the disease. The absence or low levels of the protein worsen and maintain the uncontrolled inflammation that perpetuates the disease.[13–17] Interactions between AnxA1 and FPR1 mediate IBD wound closure, and FPR2 promotes mucosal healing by regulating the trafficking and functions of leukocytes into inflamed tissue.[18–22] Ac2-26 comprises 25 amino acids of the N-terminal sequence of AnxA1 that bind to FPR1 and 2 to display equivalent biological actions to those of the full-length protein,[8,23,24] including those evoked by AnxA1 on IBD.[25–28]

According to the data, the pharmacological administration of recombinant AnxA1 (rAnxA1) or its synthetic N-terminal-related peptides could play a mandatory role in IBD therapy. Indeed, this approach has been recently tested using lipid nanoparticles loaded with rAnxA1[29] or polymeric nanoparticles loaded with Ac2-26.[27] These strategies are more effective at treating colitis in mice than free AnxA1 or Ac2-26 if locally administered, which demands nonfeasible invasive routes of administration to treat chronic patients.[26–28] A nanoparticle based on an ROS-responsive material carrying Ac2-26 was found to be effective for treating colitis via the oral route in mice because of the release of the peptide by the action of ROS at the inflammatory site.[29]

To improve the desirable oral delivery of novel drugs to treat IBD, we developed and characterized a nanostructured silica mesoporous microparticle loaded with Ac2-26 and coated it with EL30D-55 to treat IBD via the oral route. EL30D-55 is a biodegradable, inactive and pH-sensitive polymer that prevents gastric degradation and allows drug release in a pH range of 5.5 to 7.0. When dealing with IBD, EL30D-55 overcomes the limitations of gastric degradation and helps to deliver the desired molecule to inflamed intestines.[30,31] Indeed, the data herein confirmed the effectiveness of EL30D-55-coated SBA-15 containing Ac2-26 as a simple and cost-effective noninvasive approach for IBD treatment.

Materials and Methods

Materials

SBA-15 was synthesized at the Physics Institute, University of São Paulo, Brazil, according to a previous work.[32] SBA-15 silanized with the amino-functional trimethoxysilanes (APTES); Eudragit® (L30-D55; Evonik Industries AG - Rellinghauser Straße – Essen Germany); phosphotungistic acid hydrate, reagent grade (Sigma; St. Louis, USA); peptide Ac2.26 (Proteinmax- São Paulo, Brazil); ethanol were of analytical grade (Sigma; St. Louis, USA); dextran sulfate sodium (DSS, MW 40,000, Dextran Products Limited, Ontario, Canada); anti-mouse MUC-2 (Invitrogen®, Waltham, Massachusetts, USA); anti-mouse F4/80 (eBioscience™, San Diego, California, USA); anti-mouse Claudin-1 and secondary antibody anti-rabbit conjugated with HRP (Abcam Plc, Cambridge, United Kingdom); anti-mouse Ly6G (BD, Becton Dickinson, New Jersey, US); DAB Substrate Chromogen System (Dako Omnis, Agilent, Santa Clara, California, USA); anti- proliferating cell nuclear antigen (PCNA)(Santa Cruz Biotechnology, Dallas, Texas, USA); anti-CD163 (Bioss Antibodies Inc, Massachusetts, USA); Collagenase II and Collagenase IV from *Clostridium histolyticum* and bovine serum albumin (BSA) (Gibco™, New York, USA). ELISA kits anti-mouse TNF, IL-10, CXCL-1, IL-17 and IL-23 (BD OptEIA™ - BD, Becton Dickinson, New Jersey, US); isoflurane (Cristália Produto Químicos e Farmacêuticos Ltda, São Paulo, Brazil); paraformaldehyde, xilene, sodium citrate, peroxide and tris (hydroxymethyl) aminomethane (Synth® - Labsynth Produtos para Laboratórios LTDA, São Paulo, Brazil); cytochalasin D, (3-[4,5-dimethylthiazol-2-yl]-2,5 diphenyl tetrazolium bromide (MTT) (Millipore Sigma, Darmstadt, Germany); pluronic P123 (BASF, German); tetraethyl orthosilicate; Fluorescein isothiocyanate (FITC); Cyanine-5.5 NHS ester (Cy5.5 – Lumiprobe Corporation, Hunt Valley, USA); Spectra/Por® 10 mm dialysis membrane tube (500 Da) (Spectrum® Laboratories; New Brunswick, USA); J774A.1 cells (ATCC®; Washington DC, USA); Raw 264.7 and Caco-2 cells (BCRJ®; Xerém, Brazil).

Synthesis of SBA-15

SBA-15 was synthesized using 4 g of Pluronic P123 ($PEO_{20}PPO_{70}PEO_{20}$). It was dissolved in 122 g of 2 M HCl solution and kept under magnetic and mechanical stirring for 1 hour. Then, 8.6 g of tetraethyl orthosilicate was added, and the solution was stirred for 24 hours. After this process, the mixture was subjected to a 48-hour hydrothermal treatment at 100 °C in an autoclave, washed with deionized water, and dried at room temperature. The polymer template was then removed through calcination at 540 °C under N_2 for 2 hours and in air for 4 hours.

Ac2-26 was synthesized by dissolving the peptide in Milli-Q water, and then a 1:1 mixture of SBA-15:Ac2-26 was made, where 1 mg/mL of Ac2.26 was added to 1 mg of SBA-15. The mixture was dried in an oven at 35 °C until completely dry. For coating with EL30D-55, a 1:2 ratio of SBA-15-Ac2-26 and EL30D-55 was added. The material was dried in an oven at 35 °C for 4 hours and then stored in a freezer at −20 °C (Supplementary Figure 1).

Characterization of SBA-15

Dynamic light scattering (DLS) measurements were performed at room temperature on a Brookhaven DM-5000 Particle Size Analyzer (Brookhaven Instruments, NY, USA) at a wavelength of 635 nm. Data analysis was conducted using the BIC software provided with the machine. The sample was diluted to 1 mg/mL to mitigate the influence of interparticle interactions on the diffusion coefficient of the particles and, consequently, on the obtained data.

Small-angle X-ray scattering (SAXS) was performed on a NanoStar (Bruker, Buffalo, USA) instrument equipped with a microfocus Genix 3D system (Xenocs, Massachusetts, USA) and a Pilatus 300k detector (Dectris, Baden, Switzerland). The sample-to-detector distance was ~667 mm, which provided an effective range of the modulus of the transfer moment vector, $q = 4\pi\sin(\theta)/\lambda$ (where 2θ is the scattering angle and $\lambda = 1.5418$ Å is the X-ray wavelength), from 0.015 to 0.30.$^{-1}$ For the experiments, deionized water (used in the sample preparation) and the same sample from the DLS assays were measured at room temperature in a reusable quartz capillary 1.5 mm in diameter mounted on stainless steel. Powder samples of SBA-15 and SBA-15 plus peptide were placed in a sample holder between two mica sheets. The set of mica sheets was also measured for background correction purposes. Data treatment, which included azimuthal integration, background subtraction and absolute scale normalization (for the liquid sample), was performed using XSACT software by Xenocs.

The nitrogen adsorption isotherms (NAIs) were obtained with an ASAP2020 instrument (Micromeritics®, Atlanta, USA) using nitrogen gas.

Transmission Electron Microscopy – TEM

The transmission electron microscopy investigation was performed using a JEOL 2100 instrument equipped with a LaB 6 filament, operating at 200 kV. The samples were dispersed in water, and a few droplets of the suspension were transferred onto a carbon coated collodion film copper grid. For the SBA containing the peptide and the fluorophore samples (SBA-15-Ac2-26, FITC-SBA-15), a drop of a 2% tungstic acid solution was added on the grid, and rinsed after 1 minute with deionized water, for negative staining.

SBA-15 Uptake and Cytotoxicity

SBA-15 uptake into cells was analyzed by FITC labeling. For this purpose, SBA-15 silanized with APTES was used according to the protocol described by Appiah-Ntiamoah et al.[33] After labeling, SBA-15 was analyzed by SAXS measurements. The mouse macrophage Line J774A.1 was cultured and seeded in 24-well plates as previously described.[34,35] Cytochalasin D (20 µM) was added for 1 hour, and the solution was removed before treatment with FITC-SBA-15 (10 µg/mL). The cellular uptake was checked 4 and 24 hours after treatment using cell imaging (CELena® Logos Biosystem, USA), and ten fields per condition were analyzed. The percentage of phagocytic cells was quantified using ImageJ software. In addition, the effects of different concentrations of SBA-15 on macrophage cytotoxicity were assessed using the MTT assay.[36]

Murine 3D organoids and organoid-derived differentiated epithelial cells were isolated and cultured as previously described.[37,38] FITC-SBA (10 µg/mL) was added to the organoids and the apical part of the differentiated epithelial cells, and the cells were analyzed 6 days or 24 hours later, respectively.

In vitro Release of Peptide by SBA-15

The peptide Ac2-26 was dissolved in PBS (pH 7.4) to a concentration of 1.0 mg/mL. Simultaneously, 1 mg of Cy5 dye was dissolved in 1 mL of 1 mM DMSO. The peptide and Cy5 dye were mixed at a 1:10 molar ratio, and any excess dye was removed through dialysis using a 10 mm membrane with a 500 Da cutoff. The Cy5-labeled peptide was purified with Sephadex G-25 and then lyophilized. Spectrophotometry at 215 nm (Shimadzu Scientific, Marlborough, USA) confirmed the success of the labeling process. The yield of the Cy5-labeled peptide was ten vials, each containing 450 µg.

Next, the labeled peptide was incorporated into SBA-15 and used to test the release of the peptide into cells. The uptake of SBA-15-Ac2-26-Cy.5.5 and FITC-SBA-15 was measured by flow cytometry (BD, Accuri C6, USA) in mouse Raw 264.7 macrophages and Caco-2 human intestinal epithelial cells. The presence of the peptide Ac2-26Cy.5.5 was

analyzed 30 minutes, 2 hours, 6 hours and 24 hours after incubation with SBA-15-Ac2-26-Cy.5.5. Caco-2 cells were used to measure the uptake of FITC-SBA-15 after 4 and 24 hours of incubation. After the incubation, the cells were collected, washed twice and resuspended in PBS. To quantify the percentage of positive cells, at least 10,000 events were collected. The events were collected with the delimitation of the principal population of healthy cells, and the percentage was set in relation to the untreated condition.

Animals

Male C57BL6 wild-type mice aged 8–10 weeks and weighing 20–25 g were obtained from the Faculty of Pharmaceutical Sciences of the University of São Paulo. Mice were maintained under pathogen-free conditions on a 12-hour light/dark cycle at temperatures between 20 and 25 °C with free access to water and food. The protocol of the study was approved by the Ethics Committee of Animal Use of the Faculty of Pharmaceutical Sciences of the University of São Paulo (CEUA/FCF/USP; protocol n°653), following Brazilian laws on animal ethics.

In vivo and ex vivo Evaluation of SBA-15 and Ac2-26 in the Gastrointestinal Tract

The homing of SBA-15 to the TGI was evaluated by coating FITC-SBA-15 with EL30D-55. Eudragit-FITC-SBA-15 (400 µg/400 µL) was administered orally to healthy mice on Day 6. Animals were euthanized 6 or 18 hours later to withdraw the TGI. Ex vivo fluorescence images were acquired using IVIS ® Lumina LT Series III equipment (Xenogen Corp., Alameda, CA, USA) using the following parameters: excitation/emission, 465/520; automatic exposure time, F/stop 4; and binning, 4. For fluorescence intensity analysis, we selected a region of interest and normalized it to the corresponding area. The signals acquired were analyzed using Living Image Software version 4.7.2 in units of photons/s.

Experimental Colitis

Experimental colitis was induced by gavage (v.o.) of 2% DSS, which was conveyed in the water of the animals from Days 0–6, so that they received constant doses of DSS. The animals were divided into four groups: DSS, DSS + Eudragit-SBA-15 (200 µg) and DSS + Eudragit-SBA-15-Ac2.26 (200 µg), both in a final volume of 400 µL. Treatments were administered daily via the oral route between Days 6 and 9. The naive or DSS groups were manipulated as were the other groups but with the carrier solution PBS only (Supplementary Figure 2). Clinical parameters (body weight, diarrhea, and rectal bleeding) were evaluated daily (Day 0 to Day 10) to assess the evolution of colitis. The disease severity index (DAI) was calculated from the sum of the clinical parameters. On Day 10, the animals were anesthetized by isoflurane inhalation (2-chloro-2-(difluoromethoxy)-1,1,1-trifluoroethane) and euthanized. Intestinal length was evaluated, and macroscopic analyses were performed. Colon samples were collected from the ileocecal junction up to the proximity of the anus and subjected to histological (distal colon), enzymatic and flow cytometry (mid/proximal colon) analyses.

Histopathological Analysis

Fragments collected from the distal part of the colon were fixed by 24 hours of incubation in 4% paraformaldehyde for 24 hours. Histopathological analysis was performed on 4 µm sections. The samples were stained with hematoxylin and eosin solution and analyzed using an AxioCam system coupled to a Zeiss microscope (Carl Zeiss, Jena, Germany). Histopathological score analysis was performed by two analysts who were blinded to the characteristics of the intestinal tissue. The following scores were used: tissue edema, dysplasia/altered histoarchitecture, crypt edema, inflammatory infiltrates, and ulcerations. Ten photos were taken of each histological section using a 20x high-power objective, and scores were evaluated on a scale ranging from 0 to 4.

Immunohistochemistry Analysis

Colon sections were deparaffinized, hydrated and incubated with sodium citrate buffer (pH 6.0) at 96 °C for 30 minutes. Endogenous peroxidase activity was blocked with 3% hydrogen peroxide, and the sections were washed three times after each 10-minute incubation. Next, nonspecific binding sites were blocked with 1% BSA diluted in Tris-buffered saline (TBS) for one hour. The obtained sections were incubated with antibodies against Claudin-1 (1:50), MUC-2 (1:200),

PCNA (1:10) and CD163 (1:100). Afterward, the membranes were washed and incubated with a secondary antibody conjugated with HRP (1 hour, room temperature), and the signals were detected using 3.3′-diaminobenzidine. The sections were photographed using an AxioCam system coupled to a Zeiss microscope (Carl Zeiss, Jena, Germany) with a 40x high-power objective. The percentage of the area marked with Claudin-1 was quantified using ImageJ software. The results are expressed as the mean ± S.E.M. of the percentage of the marked area. MUC-2, PCNA and CD163 were quantified by using a 40× high-power objective in ten fields of the mucosal layer from the sections, and the number of positive cells was quantified for each field. The results are expressed as the mean ± S.E.M. of cells per field.

Isolation of Leukocytes from Lamina Propria and Flow Cytometry

Leukocytes from the proximal colonic lamina propria were isolated after washing with 2 mM EDTA, followed by digestion with collagenase II and IV from *Clostridium histolyticum* (1 mg/mL). The cells were washed through 40-µm strainers (Corning, Corning, NY, USA) and stained with Ly6G (PE) and F4/80 (PerCpCy5.5). Positive populations were identified by labeling with single antibodies. A minimum of 10,000 events per sample were acquired on a BD Accuri C6 Flow Cytometer (BD, Becton Dickinson, New Jersey, US). The results are expressed as percentages of positive cells normalized to controls from each experiment.

Enzyme Linked Immuno Sorbent Assay (ELISA)

A portion of 0.5 cm from the large intestine was segmented and 200 µL of ice-cold lysis buffer containing proteinase inhibitors was added and homogenize using electric homogenizer. The contents were centrifugated and the supernatant stored for protein quantification. Protein quantification was measured by Bredford reagent. ELISA was performed following the manufacturer instructions. The result was normalized to the protein concentration.

Statistical Analysis

The experimental colitis model was subjected to analysis of clinical parameters using two-way ANOVA with a subsequent Bonferroni post hoc correction. In addition, for other analyses, one-way ANOVA was utilized, followed by Tukey's post hoc test. The significance level was set at $p < 0.05$, and the results are presented as the mean ± SEM. GraphPad Prism 9.0 (San Diego, California, USA) software was used to conduct the statistical analyses.

Results

The Ac2-26 Solution is Composed of Rod-Like Particles

Ac2-26 was successfully dispersed in deionized water at a concentration of 6 mg/mL, allowing future experiments that could require higher concentrations. Interestingly, the sample is more viscous than pure water and slightly hazy, which indicates the likely existence of large aggregates, as these features are mitigated after dilution. To probe such aggregates, we proceeded with DLS assays. Figure 1A shows the obtained autocorrelation function (black filled circles), C(τ), fitted with the nonnegatively constrained least squares (NNLS) method[39] (red continuous line). From the satisfactory fitting, the size distribution weighted by intensity, volume and number was evaluated (inset of Figure 1A). There are three populations of particles with sizes of 23 ± 1 nm, 109 ± 28 nm and 58 ± 18 µm, with the first being the most numerous. Considering the results, none of these sets correspond to the peptide alone, with a molecular weight of only 3089.46 Da, as reported by the manufacturer, but its self-assembled supramolecular structure and even aggregates. It is important to realize that such analysis assumes a spherical shape for the probed objects. To confirm this feature, we performed SAXS experiments on the same sample used for DLS.

The obtained SAXS data are shown in Figure 1B (black filled circles), and they were satisfactorily fitted by the indirect Fourier transform (IFT),[40] implemented in the WIFT software. From the fitting (blue continuous line), the so-called pair distance distribution p(r) was obtained (inset of Figure 1B, blue continuous line), which provides the particle's longest length of ~23 nm where $p(r) \approx 0$), in agreement with the DLS results concerning the population with the smallest objects. Furthermore, the pair distance distribution, p(r), suggests the presence of elongated particles, for instance, with rod shapes. In this context, a test was performed in which the SAXS data were fitted with a simple cylinder model.

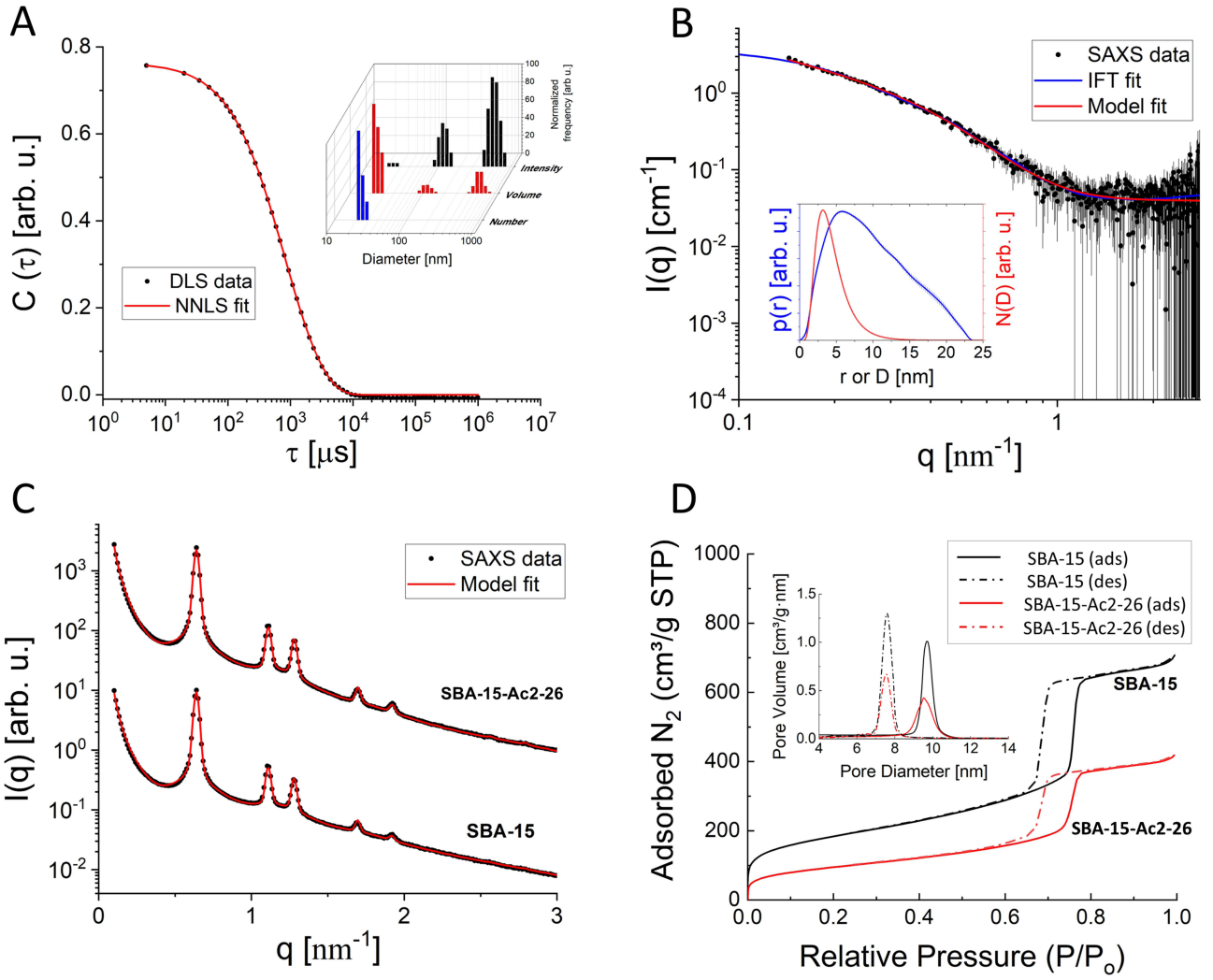

Figure 1 (**A**) Autocorrelation function (filled black circles) fitted by the NNLS method (continuous line). Inset: Hydrodynamic diameter distributions of the peptide weighted by number, volume, and intensity. (**B**) SAXS data of the peptide in solution (filled circles) fitted by the IFT method (blue continuous line) and the cylinder model (red continuous line). Inset: The obtained p(r) function, from IFT, and the size distribution function of the cylinder radius, N(D), from the model fitting. (**C**) SAXS data (filled black circles) of the pure SBA-15 and the SBA-15 incorporated with Ac2-26 (sample SBA-Ac2-26) fitted by the SBA-15 model (red continuous line). The curves were vertically shifted for a clearer visualization. (**D**) NAI data of pristine SBA-15 and the SBA-15 incorporated with Ac2-26 (sample SBA-Ac-26). Inset: Pore size distribution (PSD, adsorption and desorption).

A lognormal size distribution for the radii was also used, as in previous works.[41] The obtained satisfactory fit (Figure 1B, red continuous line) corroborates the hypothesis of a cylindrical shape. In this case, the objects have an average radius of ~3 nm, according to the obtained size distribution (inset of Figure 1B, red continuous line) and length of ~80 nm. The former value is out of the probed scale length, defined by the minimum value of the q range; thus, it cannot be precisely determined. Thus, the value indicated by the p(r) function, ~23 nm, was assumed to be the cylinder length.

Overall, the SAXS and DLS results suggested that the peptide self-assembled into rod-shaped particles.

SBA-15 is a Suitable Mesoporous Material for Anchorage Ac2-26

The percentage of peptide incorporated into SBA-15 was approximately 88.8% ± 1.2% (n=4) 88.8%, as measured by the Bradford dye-binding method. SAXS measurements were performed on powder samples of pure SBA-15 and SBA-15 containing the peptide (sample SBA-Ac-26). The obtained data are shown in Figure 1C (black-filled circles), and the obtained results are comparable to those previously reported for ordered mesoporous silica.[42–44] It is interesting to note that both curves, with and without peptide, are very similar.

To describe their structure and eventual differences, we proceeded with the data analysis using the model fully detailed by Losito et al 2021a.[43] The main fitting parameters, as well as their values, are summarized in Table 1. R and T correspond to the core radius and the shell thickness, respectively, of the core-shell cylinder modeling the mesopores, and σ_{rel} is the shared standard deviation of the log-normal size distribution of R and T. The parameter $\frac{\Delta\rho_{core}}{\Delta\rho_{shell}}$ indicates the contrast electron density of the core relative to that of the shell. Ideally, for "empty" mesopores. Otherwise, indicates the existence of some material inside the mesopores. a is the lattice parameter, and σ_a quantifies the distortion of the lattice relative to an ideal 2D-hexagonal lattice (for an ideal lattice). Finally, AP is the scale factor of the Porod term (proportional to the q^{-4} decay law) and reflects, for instance, changes in the low q region of the SAXS curve related to the presence of large aggregates, while $R_{Gpolymer}$ is the radius of gyration related to polymer-like scattering at high q originating from the synthesis of SBA-15.

As expected, both curves have similar structural parameters, except for the AP parameter. In comparison to that of pure SBA-15, its value increased ~3 times with the addition of peptide, which suggests the presence of material on the SBA-15 macroporosity. Moreover, the parameter $\Delta\rho_{core}/\Delta\rho_{shell}$ slightly increased with peptide incorporation, indicating that a fraction of the material was inside the mesopores. Considering that the percentage of peptide anchors was 87%, as

Table 1 Structural and Textural Properties of the Pristine SBA-15 Sample and the SBA-15 Incorporated with Ac2-26 (Sample SBA-Ac-26) Obtained from SAXS and NAI Techniques

Technique	Assessed Physical Parameter in Each Technique	Samples	
		SBA-15	SBA-Ac2-26
SAXS	$R\ [nm]$	4.37(1)	4.37(9)
	$T\ [nm]$	2.56(3)	2.53(2)
	$\sigma_{rel}[\%]$	7.2(2)	7.8(9)
	$\frac{\Delta\rho_{core}}{\Delta\rho_{shell}}$	0.000(1)	0.006(1)
	$a\ [nm]$	11.33(1)	11.33(1)
	$\sigma_a\ [nm]$	0.044(6)	0.041(4)
	$AP \times 10^{-8}$	7.2(7)	20.8(2)
	$R_{Gpolymer}[\mathring{A}]$	6.7(6)	8.1(5)
NAI	BET surface area $[m^2/g]$	768 (1)	342 (1)
	Decrease in surface area [%]	N/A	55
	BJH Mesopore Volume $[cm^3/g]$	1.74 (1)	0.65 (1)
	Filling/blocking Percentage [%]	N/A	62
	Mean pore diameter(ads) $[nm]$	9.4 (1)	9.5 (1)
	Mean pore diameter(des) $[nm]$	7.5 (1)	7.6 (1)
	Wall thickness $[nm]$	1.9 (1)	1.8 (1)

Notes: All uncertainties in the last digit, when exist, are presented between parentheses. R: core radius; T: shell thickness; σ_{rel}: standard deviation of the log-normal size distribution; $\frac{\Delta\rho_{core}}{\Delta\rho_{shell}}$: contrast electron density of the core relative to the shell; a: lattice; σ_a: distortion of the lattice relative to an ideal 2D-hexagonal one; AP: scale factor of the Porod term; $R_{Gpolymer}$: radius of gyration related to the polymer-like scattering. σ: sigma. Å: angstrom, wave length of the electromagnetic radiation.
Abbreviations: Ads, adsorption; Des, desorption; N/A, Not applicable.

previously discussed, most of the Ac-26, in its aggregated/self-assembled form, possibly exhibited SBA-15 macroporosity.

To obtain more information on SBA-15 pore filling by the peptide, NAI experiments were performed. The sorption results for the SBA-15 samples, pristine and loaded with Ac2-26 (peptide:silica, 1:35 wt%), are shown in Figure 1D and are similar to those reported by Zhao et al[45] for the SBA-15 material. The isotherms of both samples show hysteresis loops with sharp adsorption and desorption branches, which indicates a narrow pore size distribution (PSD). From the quantitative analysis using the Brunauer–Emmett–Teller (BET) and Barrett–Joyner–Halenda (BJH) models as well as calculations based on previous works,[46] the PSD was obtained (inset of Figure 1D) along with other useful parameters summarized in Table 1. Although the PSDs of both samples are very similar, the data presented in Table 1 show a reduction of ~55% in the surface area (internal mesopicroporosityxternal macroporosity) after the incorporation of the peptide into SBA-15. Additionally, considering the ~62% reduction in the available mesopore volume, which can indicate either filling or blocking of the pore entrance, we can conclude that the peptide is located inside the silica pores (mesopores and/or macropores). In combination with the SAXS results, the hypothesis that most of the peptides are likely to have SBA-15 macroporosity is supported. To augment this hypothesis, transmission electron microscopy (TEM) was conducted. By examining the images, focusing solely on contrast differences, there is a clear observation of channel filling in the FITC-SBA-15 sample. However, Ac2-26, an organic compound with a low molecular weight (~3 kDa), exhibits slight variation in TEM micrographs when compared with SBA-15 (Supplementary Figure 3). The possibility of increasing the peptide concentration is evident since there is still "free space" in the SBA-15 pores, with the care of preserving a homogenous distribution.

SBA-15 Does Not Cause Cytotoxicity and Releases Ac2-26

Fluorophore labeling was employed to investigate the uptake of SBA-15 and the release of Ac2-26 by SBA-15 into cells. SAXS and TEM measurements revealed the incorporation of fluorophores into SBA-15 without robust changes in the SBA-15 scattering profile (Supplementary Figures 3 and 4). Here, we show the low uptake of SBA-15 by differentiated colonic epithelial cells (Figure 2A and D, Supplementary Figure 5) and 3D colonic organoids (Figure 2B, Supplementary Figure 5), which indicates that SBA-15 may be poorly absorbed in the gut. Moreover, further flow cytometry analysis confirmed these data (Supplementary Figure 6). Nonetheless, enhanced epithelial permeability or even disruption of the epithelial barrier that occurs during gut inflammation may favor microparticle influx into tissue.

Hence, SBA-15 may be taken up by phagocytes in the inflamed tissue. Data presented in Figure 2C showed that J774 murine macrophages engulfed the microparticle by phagocytosis, as the percentage of intake was blocked by cytochalasin D with a concentration of 20 µM. The uptake of microparticles increased with time (Figure 2E and F) and did not cause cytotoxicity until 48 hours of incubation (Figure 2G). Indeed, these data corroborate previous data depicting SBA-15 as a promising drug carrier into epithelial cells in the gut and inflammatory phagocytes.[47]

To evaluate the delivery of Ac2-26 by SBA-15, Caco-2 epithelial cells were incubated with SBA-15 loading Ac2-26-Cy5.5 labeled. Flow cytometry assay detected fluorescence emitted by Ac2-26-Cy5.5 in the epithelial cells after 30 minutes of incubation, which was increased 6 hours after incubation (Figure 2H). Furthermore, similar data was found in Raw 264.7 macrophages, which also evidences the capability of SBA-15 to deliver the peptide into phagocytes (Figure 2H).

Biodistribution of Eudragit-SBA-15 in the Gastrointestinal Tract (GIT) and Peptide Release into the Gut

Notably, in vitro dissolution analysis revealed that the Ac2-26 peptide was released from Eudragit-SBA-15 in a pH solution close to that found in the duodenum (Supplementary Figure 7). Hence, to confirm whether the peptide was delivered into the gut, Eudragit-SBA-15-Ac2-26Cy.5.5 was orally administered, and the intensity of fluorescence in the GIT was measured after 3 hours of administration, which was maintained until 8 hours of analysis (Figure 3A).

To evaluate the transit of Eudragit-FITC-SBA-15 in the GIT and in the large intestine, we tracked the effects of treatment 6 and 18 hours after oral administration in mice. The signals of Eudragit-FITC-SBA-15 were detected in the

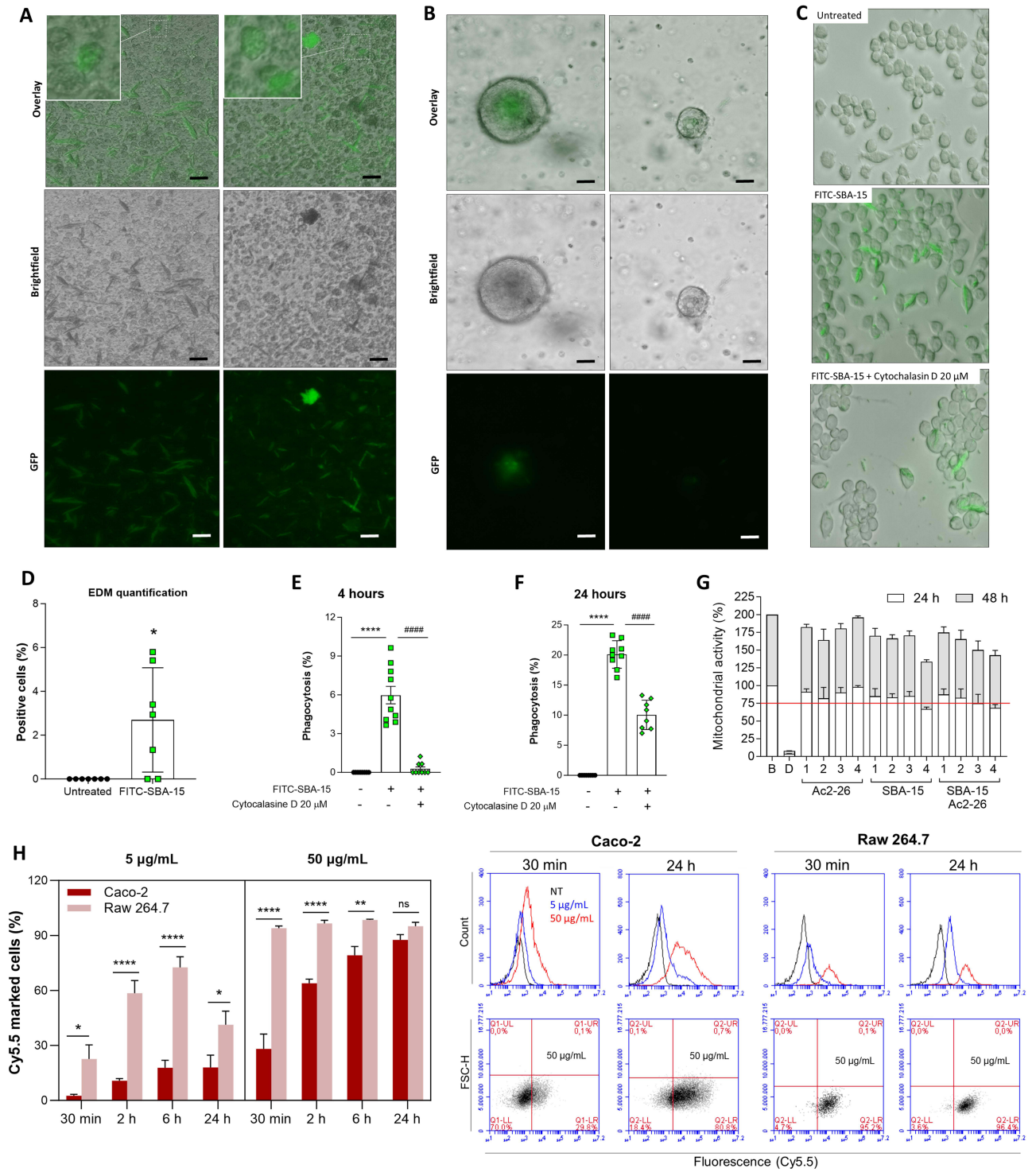

Figure 2 (**A**) Representatives pictures from differentiated EDMs treated FITC-SBA for 24 hours. In All images, green inside the cells represent microparticles internalization. (**B**) Representative pictures showed 3D murine organoid challenged with microparticles and cultured for 6 days. (**C**) Representative pictures showed macrophages J774 challenged or not with microparticles for 24 hours in presence or absent of phagocytosis inhibitors (cytochalasin (**D**). (**D**) The percentage of microparticles uptake was determined. Determined by parametric Student's *t*-test. (**E** and **F**) represent the uptake quantification of FITC-SBA after 4 hours (4h) and 24 hours (24h) after treatment. Scale bar represent 50 µm. Determined by One-Way ANOVA and Tukey multiple comparisons (**G**) Cytotoxicity by MTT assay using murine macrophages Raw 264.7. Ac2-26, SBA and Ac2-26-SBA concentrations 1, 2, 3 and 4 corresponding to 0.5, 5, 10 and 50 µg/mL respectively. Red line represents the 75% of mitochondrial activity. B, means cell incubated only with culture medium (Basal); D, means DMSO 10% treatment as positive control cytotoxicity. (**H**) Representative graph of Caco-2 or Raw 264.7 percentage of cells positive for Ac2-26-Cy5 at different time points: 30 minutes (30min), 2 hours, 6 hours and 24 hours. determined Two-Way ANOVA and Tukey multiple comparisons. The lower left side represents the Caco-2 and Raw 264.7 histogram median of fluorescence (upper line) and the percentage using forward scatter height (FSC-H) vs fluorescence emission for Cy5. Data obtained from the flow cytometry Accuri C6 software after 30 min and 24 hours. *<p 0.05, **<p 0.01 and ****p< 0.0001. $^{\#\#\#\#}$p< 0.0001.

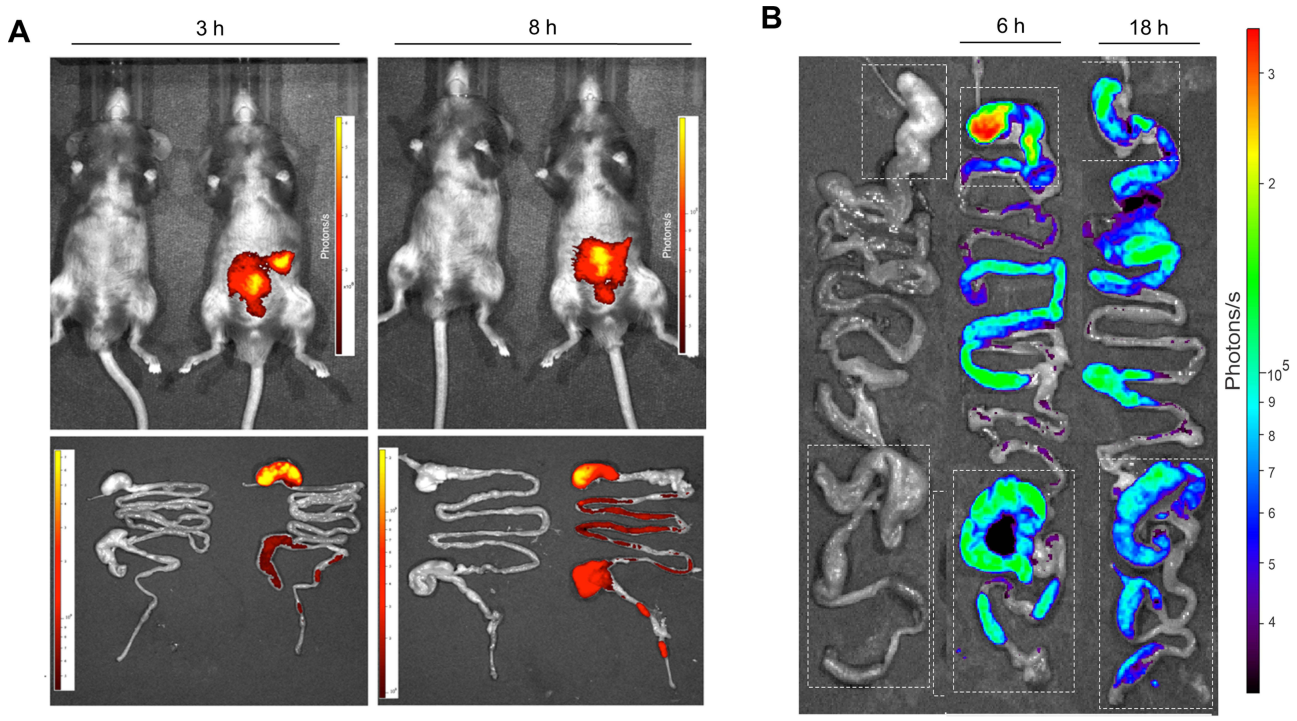

Figure 3 Biodistribution along the TGI of Eudragit-SBA-Ac2-26Cy5.5 Eudragit-FITC-SBA-15. Mice were treated orally and the intensity of the distribution is represented by photons/s. (**A**) Eudragit-SBA-Ac2-26Cy5.5 distribution was analyzed after 3 hours and 8 hours in vivo (top) and the TGI analyzed separately ex vivo (botton) at the same time points. The yellow color represents the higher intensity in the tissue. (**B**) Eudragit-FITC-SBA-15 biodistribution ex vivo along the TGI after 6 hours and 18 hours. The red color represents the higher intensity in the tissue. The white square on the top is representing the stomach portion. The white square on the bottom is representing the large intestine portion.

small and large intestines at 6 hours and 18 hours after administration, respectively (Figure 3B). Associated data obtained showed that Eudragit-SBA-15 remains in the GIT for at least 18 hours, which may lead to sustained release of the peptide into the gut, suggesting that further analysis of the therapeutic efficacy of Eudragit-SBA-15-Ac2-26 via the oral route on IBD is needed.

Eudragit-SBA-15-Ac2-26 Reduces Clinical Symptoms and Inflammation in the Gut

DSS-induced colitis is a standard model of experimental IBD.[48] The oral administration of DSS triggers the peak of the disease on Day 6, and the withdrawal of DSS promotes the initial recovery of tissue on Day 10.[16,22,29,49] Hence, oral Eudragit-SBA-15-Ac2-26 treatment started at the peak of the disease (Day 6) and was maintained at the beginning of the recovery phase (Day 10). Treatments were performed once a day based on the TGI distribution of SBA-15 and peptide release. The data obtained showed that oral administration of Eudragit-SBA-15-Ac2-26 prevented weight loss and induced colon length recovery, leading to a decreased DAI (Figure 4A–C). Moreover, the treatment inhibited the influx of neutrophils and macrophages into the inflamed gut, reduced the secretion of the inflammatory cytokines TNF-A and CXCL-1, and enhanced the secretion of the anti-inflammatory cytokine IL-10 (Figure 4D–H). The beneficial effects of the treatment were due to Ac2-26 loading, as treatment with Eudragit-SBA-15 did not prevent clinical symptoms or inflammation (Figure 4A–H).

Eudragit-SBA-15-Ac2-26 Improves the Gut Histoarchitecture

Histological analysis of the tissue revealed that DSS administration induced ulcers, crypt abscesses, vacuolar hydropic degeneration, submucosal edema, and massive mucosal/submucosal inflammatory cell infiltration. These alterations were reduced, and the colonic histological architecture was recovered by oral treatment with Eudragit-SBA-15-Ac2-26 (Figure 5A).

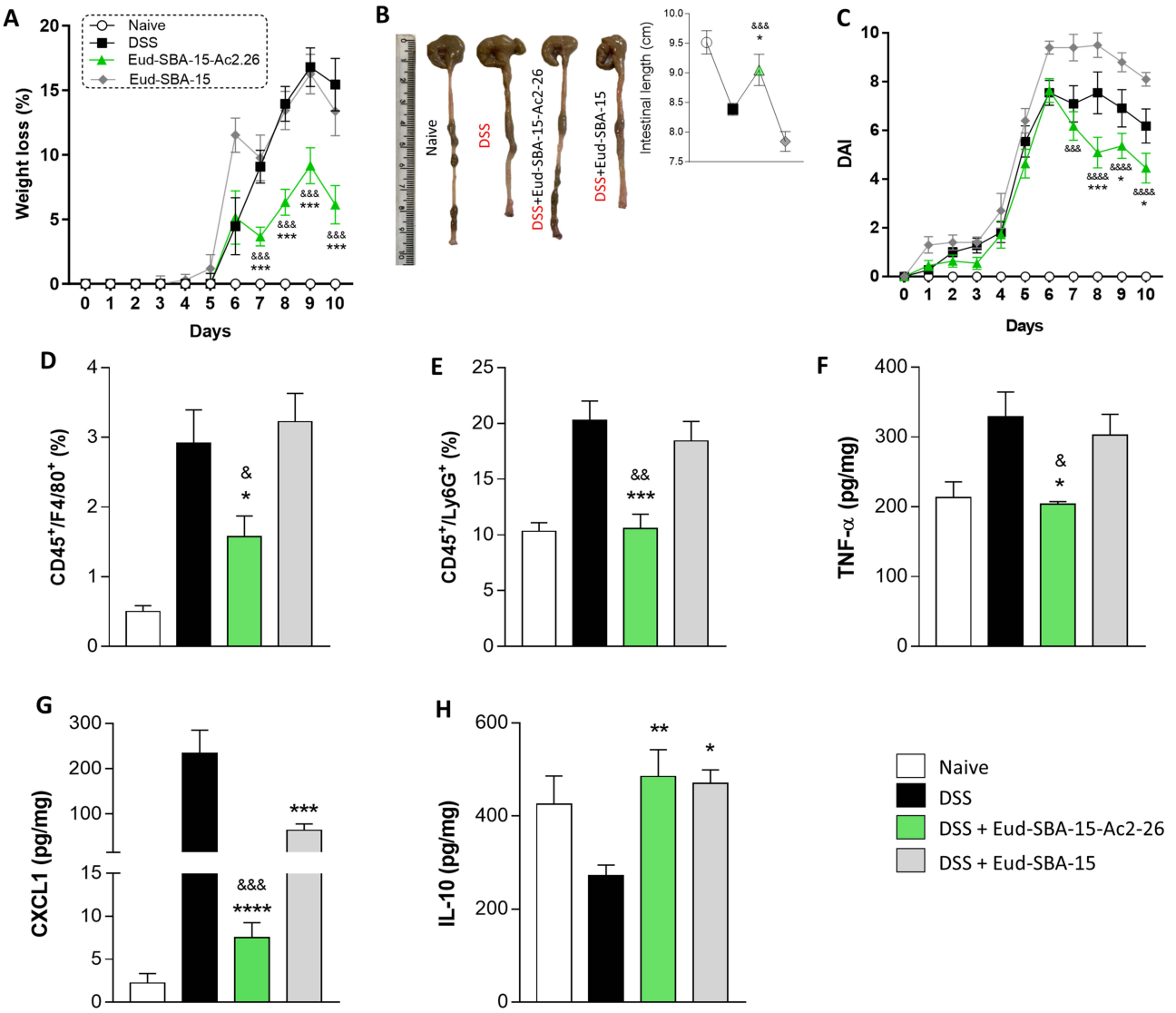

Figure 4 Clinical, cellular and secretory profile of DSS-induced colitis mice treated with Eudragit-SBA or Eudragit-SBA-Ac2-16. (**A**) Percentage of body weight loss; (**B**) Anatomic evaluation of the colon and length measure; (**C**) DAI; (**D**) Percentage of macrophages isolated from lamina propria ($CD45^+/F4/80^+$); (**E**) Percentage of neutrophils isolated from lamina propria ($CD45^+/Ly6G^+$); (**F**) TNF-α; G CXCL-1; (**H**) IL-10. n = 10 mice/group. *p < 0.05, **p < 0.01, ***p< 0.001, ****p<0.0001 vs DSS. $^{\&}$p < 0.05, $^{\&\&}$p < 0.01, $^{\&\&\&}$p< 0.001, $^{\&\&\&\&}$p<0.0001 vs Eudragit-SBA-15.

Immunohistochemical analysis was carried out to determine the mechanisms involved in the protection of the gut architecture caused by Eudragit-SBA-15-Ac2-26 treatment. DSS administration decreased the expression of claudin-1, a major component of tight junctions that is essential for epithelial cell barrier integrity; reduced the expression of mucin-2, which is associated with goblet cells, leading to impaired mucus secretion; reduced epithelial cell proliferation; and reduced the number of anti-inflammatory M2 macrophages in the tissue. Oral treatment with Eudragit-SBA-15-Ac2-26 reversed all the effects on the tissue architecture (Figure 5B–E).

Discussion

The oral route is the most preferred route for drug administration to treat IBD because it is not invasive, allows high patient compliance and flexibility in dose adjustment, and delivers the drug directly to the colonic region.[48] Nonetheless, the bioavailability of small molecules and proteins is poor after oral route administration, and suitable pharmaceutical technical approaches are required to prevent bacterial and enzyme-rich environments and different pH values in the gastrointestinal system.[48] Based on the robust beneficial effects of AnxA1 on IBD, we inferred that the AnxA1 mimetic

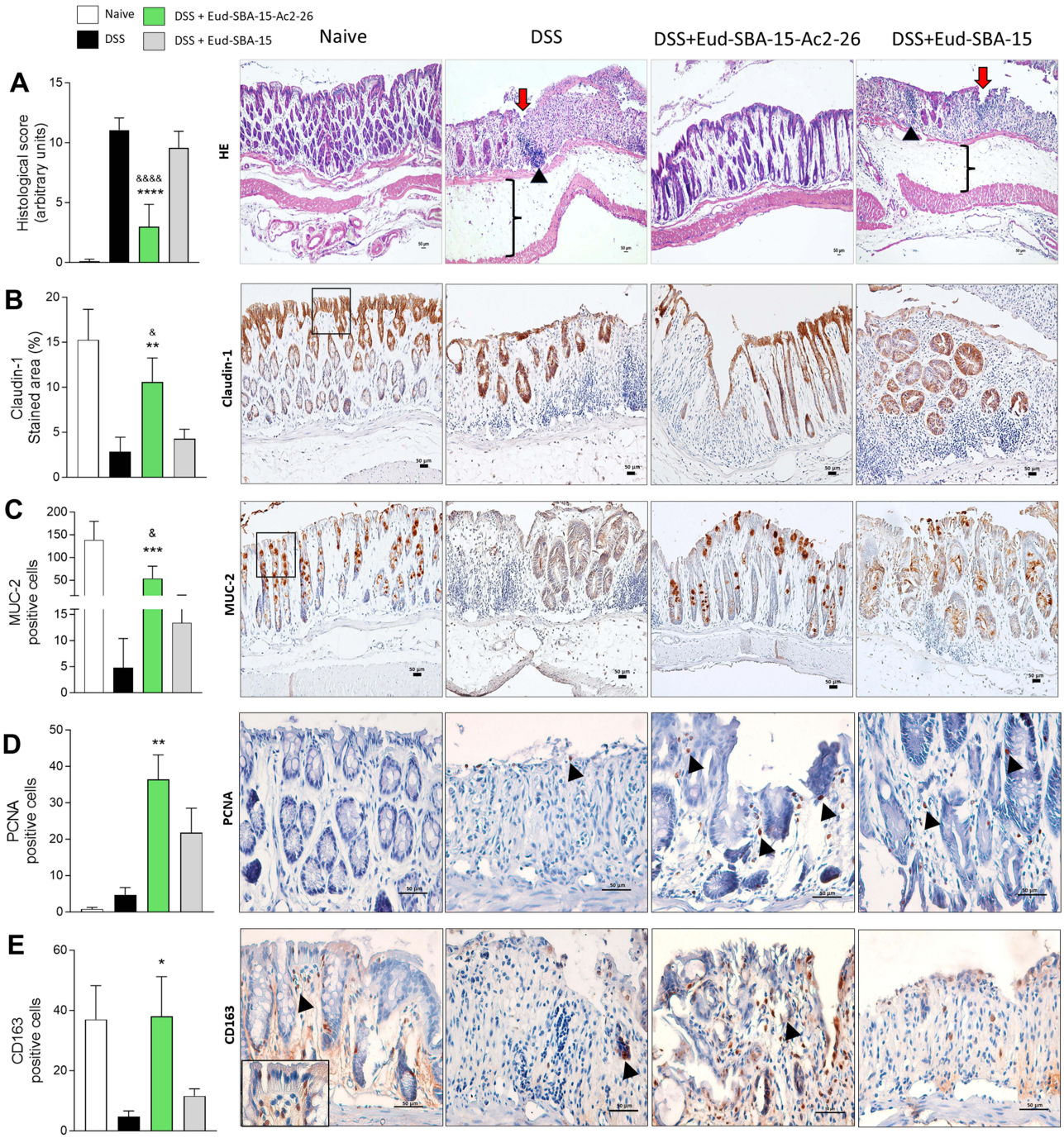

Figure 5 Histopathological sections performed with HE dyes. (**A**) Histopathological score represented by arbitrary units. The sections were blindly evaluated and considered alterations were highlighted. Tissue edema (square brackets), inflammatory infiltrates (black arrow head) and ulcerations (red arrow). Naïve section presenting normal histoarchitecture. Mice colon sections submitted to IHC. (**B**) Representative sections and percentage (%) of marked area for Claudin-1 marker. Black square represents the apical region. (**C**) Representative sections and, number of positive cells per field for MUC-2 marker. Black square represents the apical region. (**D**) Representative sections and, number of positive cells per slide for PCNA marker. Black arrow heads indicating positive cells. (**E**) Representative sections and number of positive cells per field for CD163 marker. Black arrow heads indicating positive cells. n = 10 mice/group. Scale bar: 50 μm. Sections: 4 μm. *p < 0.05, **p < 0.01, ***p< 0.001, ****p < 0.0001 vs DSS. $^{\&}$p < 0.05, $^{\&\&\&\&}$p < 0.0001 vs DSS + Eudragit-SBA-15.

peptide Ac2-26 could be incorporated into SBA-15 ordered mesoporous silica microparticles and that polymer coverage via the well-known Eudragit® (L30 D55 polymer, Evonik) could protect SBA-15-Ac2-26 from unwanted damage caused by TGI to deliver Ac2-26 into the inflamed colon.

SBA-15 is a highly thermic, hydrothermal, and mechanic-resistant material[45] that can resist pH and enzymatic reactions [46]. The structural components of SBA-15 contain many essential sylanol groups (Si-OH)[45,50] to bond substances in its structure. SBA-15 also has a large surface area, large pore volume, and narrow mesoporous pore size distribution of approximately 10 nm. Together, these properties allow the safe transport of small molecules through the TGI.[51–56] In fact, by modeling the SAXS data, in combination with the NAI results, it was possible to conclude that a fraction of the Ac2-26 peptide was loaded into the SBA-15 mesopores. In contrast, the remaining amount is on the silica surface, a similar scenario observed in previous studies,[44,57] in which the authors loaded proteins instead of peptides. As suggested by Rasmussen et al,[58] the biological content of the SBA-15 macroporosity is still being protected against harsh environmental conditions such as the TGI.

Positively charged molecules can undergo electrostatic interactions with anionic components such as glycoproteins expressed on epithelial cells. This results in charge neutralization and alteration of tight junction permeability, allowing the transport of positively charged molecules.[59] For this reason, SBA-Ac2-26 was further covered with Eudragit®, a pH-responsive anionic copolymer produced from methyl methacrylate and methacrylic acid. It exhibits pH-dependent solubility characteristics, remaining stable under acidic conditions but dissolving at basic pH (pH >7.0)[60] to facilitate drug release, which can start in the distal ileum under physiological conditions. Eudragit is an efficient drug carrier in the lower pH of the inflamed gut, as it carries a significant negative charge,[61] enabling its preferential absorption to sites of inflammation. Imaging tomography analysis confirmed that Eudragit-SBA-15 administered orally remained in the GIT for an extended period and was suitable for delivering drugs to the gut. Moreover, Eudragit-SBA-15 uptake by in vitro gut epithelial cells in two- or three-dimensional cell models was deficient, reinforcing the hypothesis that SBA-15 is not absorbed in the gut and can be excreted by feces.[47] Further data revealed that Eudragit-SBA-15 is a suitable platform for the delivery of the peptide into the gut, as Ac2-26 was detected in the epithelium after in vitro incubation with SBA-15-Ac2-26, and Eudragit-SBA-15 delivered Ac2-26 into the gut for an extended period after oral administration.

The inflammatory environment disrupts the intestinal barrier in IBD, resulting in increased permeability, allowing the leakage of nanoparticle-based therapies to the lamina propria and subsequent engulfment by phagocytes.[62–64] This may be a suitable mechanism of SBA-15-Ac2-26 in IBD, as we confirmed that macrophages efficiently phagocytose SBA-15.

The beneficial effects of Ac2-26 on IBD symptoms are related to its binding to FPR1 on the inflamed epithelium.[25,26] Moreover, AnxA1 is highly expressed by neutrophils and macrophages in the lamina propria and mediates efferocytosis via FPR2 agonism.[16,22] Ac2-26 acts similar to AnxA1, binding to both receptors for downstream anti-inflammatory and tissue repair through intracellular pathways and impairing the migration of macrophages and neutrophil to the site of the inflammation.[65] These concepts can be applied to SBA-15 distribution and the biological response of Ac2-26 to oral treatment of colitis. The treatment promoted rapid beneficial effects, as detected by the marked reduction in weight loss 24 hours after the first treatment, which was sustained for the following three administrations once a day during the recovery phase of the disease. The effectiveness of oral treatment for colitis could not be compared to that of free Ac2-26 administration due to the poor bioavailability of peptides after oral intake.[66] On the 10th day of the disease, the treatment inhibited the influx of neutrophils and monocytes into inflamed tissue and reduced the levels of proinflammatory cytokines secreted in the tissue. The latter effect could reflect the lower number of inflammatory cells. Indeed, Ac2-26, similar to AnxA1, detaches adhered cells to endothelial cells, thus limiting their trafficking to inflamed sites;[67–69] nonetheless, Ac2-26 inhibits the secretion of proinflammatory cytokines via transcriptional and posttranscriptional pathways.[28,70] Conversely, the levels of the anti-inflammatory and pro-resolution cytokine IL-10 were enhanced by the treatment, which was consistent with the high levels of anti-inflammatory CD163 M2 macrophages in the tissues of the treated mice. Ac2-26 is a recognized resolvin peptide that polarizes M2 macrophages and induces neutrophil apoptosis to further phagocytose M2 macrophages.[27,28,67–69]

In addition to reducing inflammation, Eudragit-SBA-15-Ac2-26 treatment promoted tissue repair by rescuing tight adhesion molecule and claudin-1 expression and promoting epithelial cell proliferation. AnxA1, similar to Ac2-26, induces epithelial repair in different models, and the underlying mechanisms involve binding to FPR1/FPR2 receptors downstream of the ERK1/2 phosphorylation pathway and inhibition of RhoA–ROCK signaling.[27,71–77] Phosphorylated AnxA1 downstream of ERK1/2 is clearly involved in mucin secretion and claudin-1 expression, as ERK1/2 blocks AnxA1 activity in uterine epithelial cells and conjunctival goblet cells.[76,78]

Conclusion

Here, we designed a polymer-covered microparticle containing the anti-inflammatory peptide Ac2-26 as a platform for targeted drug delivery to the inflamed colon via oral administration. This concept is based on the high incorporation of small molecules into mesoporous microparticles, which polymers can cover to protect them from the adverse effects of TGIs on drug delivery. Indeed, approximately 88% of the Ac2-26 peptide was incorporated, and massive peptide release occurred at a pH close to that of the gut microenvironment, suggesting that the peptide could be effectively protected from premature release until it reached the ileum and colon. Further data corroborated the platform's efficiency, as Eudragit-SBA-15 reached the large intestine in 18 hours and delivered the peptide to the gut, and clinical colitis symptom recovery was detected in the first 24 hours of treatment. After four doses, once a day, the inflamed tissue was recovered, demonstrating the anti-inflammatory and tissue repair effects of the peptide. Therefore, this platform holds promise, particularly for safeguarding and delivering Ac2-26 to the inflamed colon to trigger distinct intracellular pathways, which are recognized as underlying mechanisms of AnxA1 protection in IBD.

Abbreviations

IBD, inflammatory bowel diseases; AnxA1, Annexin A1; EL30D-55, Eudragit® L30-D55; SBA-15, Santa Barbara Amorphous 15; UC, ulcerative colitis; CD, Crohn's disease; FPR1, formyl peptide receptor 1; FPR2, formyl peptide receptor 2; ROS, reactive oxygen species; DSS, dextran sulfate sodium; APTES, amino-functional trimethoxysilanes; DLS, Dynamic Light Scattering, SAXS, Small-angle X-ray Scattering; NAI, nitrogen adsorption isotherms; FITC, Fluorescein isothiocyanate; Cy5.5, Cyanine-5.5; MTT, (3-[4,5-dimethylthiazol-2-yl]-2,5 diphenyl tetrazolium bromide; PBS, phosphate buffer saline; TGI, gastrointestinal tract; ANOVA, analysis of variance; SEM, standard deviation of mean.

Acknowledgments

This work was supported by FAPESP (Fundação de Amparo à Pesquisa do Estado de São Paulo), grant numbers 2017/17844-8, 2019/07007-7, 2022/11602-0, 2019/12301-1. S.H.P.F., M.C.A. Fantini are researcher fellows of the CNPq (Conselho Nacional de Pesquisa, Brazil); M.F.B. is a PhD fellow of the FAPESP, grant number 2018/26383-7. CAPES (Coordenação de Aperfeiçoamento de Pessoal de Nível Superior) supported the Graduation Program on Pharmacy – Pathophysiology and Toxicology. A part of this work was supported by the intramural funds of University of Massachusetts- Lowell (to SD) and Leona M. and Harry B. Helmsley Charitable Trust (to SD and IMS). The authors thank Larissa Otubo, PhD from the Instituto de Pesquisas Energéticas e Nucleares, IPEN/CNEN, São Paulo, Brazil, for the pivotal support on TEM experiments.

Disclosure

The authors declare no conflicts of interest in this work.

References

1. Burisch J, Zhao M, Odes S, et al. The cost of inflammatory bowel disease in high-income settings: a lancet gastroenterology & hepatology commission. *Lancet Gastroenterol Hepatol*. 2023;8(5):458–492. doi:10.1016/S2468-1253(23)00003-1
2. Xavier RJ, Podolsky DK. Unravelling the pathogenesis of inflammatory bowel disease. *Nature*. 2007;448(7152):427–434. doi:10.1038/nature06005
3. Laredo V, García-Mateo S, Martínez-Domínguez SJ, López de la Cruz J, Gargallo-Puyuelo CJ, Gomollón F. Risk of cancer in patients with inflammatory bowel diseases and keys for patient management. *Cancers*. 2023;15(3):871. doi:10.3390/cancers15030871
4. Spinelli A, Bonovas S, Burisch J, et al. ECCO Guidelines on therapeutics in ulcerative colitis: surgical treatment. *J Crohn's Colitis*. 2022;16(2):179–189. doi:10.1093/ecco-jcc/jjab177
5. Kotla NG, Rochev Y. IBD disease-modifying therapies: insights from emerging therapeutics. *Trends Mol Med*. 2023;29(3):241–253. doi:10.1016/j.molmed.2023.01.001
6. Flower RJ, Rothwell NJ. Lipocortin-1: cellular mechanisms and clinical relevance. *Trends Pharmacol Sci*. 1994;15(3). doi:10.1016/0165-6147(94)90281-X
7. Moss SE, Morgan RO. The annexins. *Genome Biol*. 2004;5(4):219. doi:10.1186/gb-2004-5-4-219
8. Perretti M, D'Acquisto F. Annexin A1 and glucocorticoids as effectors of the resolution of inflammation. *Nat Rev Immunol*. 2009. doi:10.1038/nri2470
9. Perretti M, Dalli J. Resolution pharmacology: focus on pro-resolving annexin A1 and lipid mediators for therapeutic innovation in inflammation. *Annu Rev Pharmacol Toxicol*. 2023;63(1):449–469. doi:10.1146/annurev-pharmtox-051821-042743
10. Machado ID, Spatti M, Hastreiter A, et al. Annexin A1 Is a physiological modulator of neutrophil maturation and recirculation acting on the CXCR4/CXCL12 Pathway. *J Cell Physiol*. 2016;231(11):2418–2427. doi:10.1002/jcp.25346

11. Sheikh M, Solito E. Annexin A1: uncovering the many talents of an old protein. *Int J Mol Sci*. 2018;19(4):1045. doi:10.3390/ijms19041045
12. Foo SL, Yap G, Cui J, Lim LHK. Annexin-A1 – a Blessing Or A Curse In Cancer? *Trends Mol Med*. 2019;25(4):315–327. doi:10.1016/j.molmed.2019.02.004
13. Vergnolle N, Comera C, Bueno L. Annexin 1 is overexpressed and specifically secreted during experimentally induced colitis in rats. *Eur J Biochem*. 1995;232(2):603–610. doi:10.1111/j.1432-1033.1995.tb20850.x
14. Vergnolle N, Pagés P, Guimbaud R, et al. Annexin 1 is secreted in situ during ulcerative colitis in humans. *Inflamm Bowel Dis*. 2004;10(5):584–592. doi:10.1097/00054725-200409000-00013
15. Sena A, Grishina I, Thai A, et al. Dysregulation of Anti-Inflammatory Annexin A1 expression in progressive crohns disease. *PLoS One*. 2013. doi:10.1371/journal.pone.0076969
16. de Paula-Silva M, Barrios BE, Macció-Maretto L, et al. Role of the protein annexin A1 on the efficacy of anti-TNF treatment in a murine model of acute colitis. *Biochem Pharmacol*. 2016;115:104–113. doi:10.1016/j.bcp.2016.06.012
17. Reischl S, Troger J, Jesinghaus M, et al. Annexin A1 expression capacity as a determinant for disease severity in crohn's disease. *Dig Dis*. 2020;38(5):398–407. doi:10.1159/000505910
18. Babbin BA, Laukoetter MG, Nava P, et al. Annexin A1 regulates intestinal mucosal injury, inflammation, and repair. *J Immunol*. 2008;181(7):5035–5044. doi:10.4049/jimmunol.181.7.5035
19. Wentworth CC, Jones RM, Kwon YM, Nusrat A, Neish AS. Commensal-epithelial signaling mediated via formyl peptide receptors. *Am J Pathol*. 2010;177(6):2782–2790. doi:10.2353/ajpath.2010.100529
20. Vong L, Ferraz JGP, Dufton N, et al. Up-Regulation of Annexin-A1 and Lipoxin A4 in Individuals with Ulcerative Colitis May Promote Mucosal Homeostasis. *PLoS One*. 2012;7(6):e39244. doi:10.1371/journal.pone.0039244
21. Birkl D, O'Leary MN, Quiros M, et al. Formyl peptide receptor 2 regulates monocyte recruitment to promote intestinal mucosal wound repair. *FASEB J*. 2019;33(12):13632–13643. doi:10.1096/fj.201901163R
22. de Paula-Silva M, da Rocha GHO, Broering MF, et al. Formyl peptide receptors and Annexin A1: complementary mechanisms to infliximab in murine experimental colitis and crohn's disease. *Front Immunol*. 2021:12. doi:10.3389/fimmu.2021.714138
23. Galvão I, Vago JP, Barroso LC, et al. Annexin A1 promotes timely resolution of inflammation in murine gout. *Eur J Immunol*. 2017;47(3):585–596. doi:10.1002/eji.201646551
24. Alhasan H, Terkawi MA, Matsumae G, et al. Inhibitory role of Annexin A1 in pathological bone resorption and therapeutic implications in periprosthetic osteolysis. *Nat Commun*. 2022;13(1):3919. doi:10.1038/s41467-022-31646-0
25. Leoni G, Alam A, Neumann P-A, et al. Annexin A1, formyl peptide receptor, and NOX1 orchestrate epithelial repair. *J Clin Invest*. 2013;123(1):443–454. doi:10.1172/JCI65831
26. Leoni G, Gripentrog J, Lord C, et al. Human neutrophil formyl peptide receptor phosphorylation and the mucosal inflammatory response. *J Leukoc Biol*. 2015;97(1):87–101. doi:10.1189/jlb.4a0314-153r
27. Li C, Zhao Y, Cheng J, et al. A proresolving peptide nanotherapy for site-specific treatment of inflammatory bowel disease by regulating proinflammatory microenvironment and gut microbiota. *Adv Sci*. 2019;6(18). doi:10.1002/advs.201900610
28. Reischl S, Lee JH, Miltschitzky JRE, et al. Ac2-26-nanoparticles induce resolution of intestinal inflammation and anastomotic healing via inhibition of NF-κB signaling in a model of perioperative colitis. *Inflamm Bowel Dis*. 2021;27(9):1379–1393. doi:10.1093/ibd/izab008
29. Broering MF, Leão M, da Rocha GHO, et al. Development of Annexin A1-surface-functionalized metal-complex multi-wall lipid core nanocapsules and effectiveness on experimental colitis. *Eur J Pharm Biopharm*. 2022;181:49–59. doi:10.1016/j.ejpb.2022.10.022
30. Patra CN, Priya R, Swain S, Kumar Jena G, Panigrahi KC, Ghose D. Pharmaceutical significance of Eudragit: a review. *Futur J Pharm Sci*. 2017;3(1):33–45. doi:10.1016/j.fjps.2017.02.001
31. Gao C, Yu S, Zhang X, et al. Dual Functional Eudragit® S100/L30D-55 and PLGA Colon-Targeted Nanoparticles of Iridoid Glycoside for Improved Treatment of Induced Ulcerative Colitis. *Int J Nanomed*. 2021;16:1405–1422. doi:10.2147/IJN.S291090
32. Matos JR, Mercuri LP, Kruk M, Jaroniec M. Toward the synthesis of extra-large-pore MCM-41 analogues. *Chem Mater*. 2001;13(5):1726–1731. doi:10.1021/cm000964p
33. Appiah-Ntiamoah R, Chung WJ, Kim H. A highly selective SBA-15 supported fluorescent "turn-on" sensor for the fluoride anion. *New J Chem*. 2015;39(7):5570–5579. doi:10.1039/c5nj00495k
34. Sayed IM, Ibeawuchi SR, Lie D, et al. The interaction of enteric bacterial effectors with the host engulfment pathway control innate immune responses. *Gut Microbes*. 2021;13(1). doi:10.1080/19490976.2021.1991776
35. Das S, Sarkar A, Choudhury SS, et al. Engulfment and cell motility protein 1 (ELMO1) has an essential role in the internalization of salmonella typhimurium into enteric macrophages that impact disease outcome. *Cmgh*. 2015;1(3):311–324. doi:10.1016/j.jcmgh.2015.02.003
36. van Meerloo J, Kaspers GJL, Cloos J. Cell sensitivity assays: the MTT ASSAY. *In*. 2011:237–245. doi:10.1007/978-1-61779-080-5_20
37. Sayed IM, Sahan AZ, Venkova T, et al. Helicobacter pylori infection downregulates the DNA glycosylase NEIL2, resulting in increased genome damage and inflammation in gastric epithelial cells. *J Biol Chem*. 2020;295(32):11082–11098. doi:10.1074/jbc.ra119.009981
38. Sharma A, Lee J, Fonseca AG, et al. E-cigarettes compromise the gut barrier and trigger inflammation. *iScience*. 2021;24(2):102035. doi:10.1016/j.isci.2021.102035
39. Morrison ID, Grabowski EF, Herb CA. Improved techniques for particle size determination by quasi-elastic light scattering. *Langmuir*. 1985;1(4):496–501. doi:10.1021/la00064a016
40. Glatter O. Data evaluation in small angle scattering: calculation of the radial electron density distribution by means of indirect Fourier transformation. *Acta Phys Austriaca*. 1977;47(1–2):83–102.
41. Pinto Oliveira CL. Investigating macromolecular complexes in solution by small angle X-ray scattering. In *Current Trends in X-Ray Crystallography*. InTech; 2011. doi10.5772/30730
42. Martinez RM, Oseliero Filho PL, Gerbelli BB, et al. Influence of the mixtures of vegetable oil and vitamin E over the microstructure and rheology of organogels. *Gels*. 2022;8(1):36. doi:10.3390/gels8010036
43. Losito DW, Lopes PS, Ueoka AR, et al. Biocomposites based on SBA-15 and papain: characterization, enzymatic activity and cytotoxicity evaluation. *Microporous Mesoporous Mater*. 2021;325:111316. doi:10.1016/j.micromeso.2021.111316
44. Losito DW, de Araujo DR, Bezzon VDN, et al. Mesoporous Silica–Fe3O4 nanoparticle composites as potential drug carriers. *ACS Appl Nano Mater*. 2021;4(12):13363–13378. doi:10.1021/acsanm.1c02861

45. Zhao D, Feng J, Huo Q, et al. Triblock copolymer syntheses of mesoporous silica with periodic 50 to 300 Angstrom Pores. *Science*. 1998;279 (5350):548–552. doi:10.1126/science.279.5350.548
46. Kruk M, Jaroniec M, Ko CH, Ryoo R. Characterization of the Porous Structure of SBA-15. *Chem Mater*. 2000;12(7):1961–1968. doi:10.1021/cm000164e
47. Li L, Liu T, Fu C, Tan L, Meng X, Liu H. Biodistribution, excretion, and toxicity of mesoporous silica nanoparticles after oral administration depend on their shape. *Nanomed Nanotechnol Biol Med*. 2015;11(8):1915–1924. doi:10.1016/j.nano.2015.07.004
48. Zhang F, Du Y, Zheng J, et al. Oral Administration of Multistage Albumin Nanomedicine Depots (MANDs) for Targeted Efficient Alleviation of Chronic Inflammatory Diseases. *Adv Funct Mater*. 2023;33(9):2211644. doi:10.1002/adfm.202211644
49. Mariano-Neto F, Matos JR, Cides da Silva LC, et al. Physical properties of ordered mesoporous SBA-15 silica as immunological adjuvant. *J Phys D Appl Phys*. 2014;47(42):425402. doi:10.1088/0022-3727/47/42/425402
50. Zhao D, Huo Q, Feng J, Chmelka BF, Stucky GD. Nonionic triblock and star diblock copolymer and oligomeric surfactant syntheses of highly ordered, hydrothermally stable, mesoporous silica structures. *J Am Chem Soc*. 1998;120(24):6024–6036. doi:10.1021/ja974025i
51. Scaramuzzi K, Oliveira DCA, Carvalho LV, et al. Nanostructured SBA-15 silica as an adjuvant in immunizations with hepatitis B vaccine. *Einstein*. 2011;9(4):436–441. doi:10.1590/s1679-45082011ao2162
52. Xu C, Lei C, Yu C. Mesoporous Silica Nanoparticles for Protein Protection and Delivery. *Front Chem*. 2019;7. doi:10.3389/fchem.2019.00290
53. Mechler-Dreibi ML, Almeida HMS, Sonalio K, et al. Oral vaccination of piglets against Mycoplasma hyopneumoniae using silica SBA-15 as an adjuvant effectively reduced consolidation lung lesions at slaughter. *Sci Rep*. 2021;11(1):22377. doi:10.1038/s41598-021-01883-2
54. Rosenholm JM, Sahlgren C, Lindén M. Towards multifunctional, targeted drug delivery systems using mesoporous silica nanoparticles – opportunities & challenges. *Nanoscale*. 2010;2(10):1870. doi:10.1039/c0nr00156b
55. Lu J, Liong M, Li Z, Zink JI, Tamanoi F. Biocompatibility, biodistribution, and drug-delivery efficiency of mesoporous silica nanoparticles for cancer therapy in animals. *Small*. 2010;6(16):1794–1805. doi:10.1002/smll.201000538
56. Sarkar S, Ekbal Kabir M, Kalita J, Manna P. Mesoporous silica nanoparticles: drug delivery vehicles for antidiabetic molecules. *ChemBioChem*. 2023;24(7). doi:10.1002/cbic.202200672
57. Trezena AG, Oseliero Filho PL, Cides da Silva LC, et al. Adjuvant effect of mesoporous silica SBA-15 on anti-diphtheria and anti-tetanus humoral immune response. *Biologicals*. 2022;80:18–26. doi:10.1016/j.biologicals.2022.10.001
58. Rasmussen MK, Kardjilov N, Oliveira CLP, et al. 3D visualisation of hepatitis B vaccine in the oral delivery vehicle SBA-15. *Sci Rep*. 2019;9 (1):6106. doi:10.1038/s41598-019-42645-5
59. Bannunah AM, Vllasaliu D, Lord J, Stolnik S. Mechanisms of nanoparticle internalization and transport across an intestinal epithelial cell model: effect of size and surface charge. *Mol Pharm*. 2014;11(12):4363–4373. doi:10.1021/mp500439c
60. Thakral S, Thakral NK, Majumdar DK. Eudragit®: a technology evaluation. *Expert Opin Drug Deliv*. 2013;10(1):131–149. doi:10.1517/17425247.2013.736962
61. Barbosa JAC, Abdelsadig MSE, Conway BR, Merchant HA. Using zeta potential to study the ionisation behaviour of polymers employed in modified-release dosage forms and estimating their pKa. *Int J Pharm X*. 2019;1:100024. doi:10.1016/j.ijpx.2019.100024
62. Beloqui A, Coco R, Alhouayek M, et al. Budesonide-loaded nanostructured lipid carriers reduce inflammation in murine DSS-induced colitis. *Int J Pharm*. 2013;454(2). doi:10.1016/j.ijpharm.2013.05.017
63. Hua S. Advances in oral drug delivery for regional targeting in the gastrointestinal tract - influence of physiological, pathophysiological and pharmaceutical factors. *Front Pharmacol*. 2020;11:1–22. doi:10.3389/fphar.2020.00524
64. Mitchell MJ, Billingsley MM, Haley RM, Wechsler ME, Peppas NA, Langer R. Engineering precision nanoparticles for drug delivery. *Nat Rev Drug Discov*. 2021;20(2):101–124. doi:10.1038/s41573-020-0090-8
65. Cooray SN, Gobbetti T, Montero-Melendez T, et al. Ligand-specific conformational change of the G-protein-coupled receptor ALX/FPR2 determines proresolving functional responses. *Proc Natl Acad Sci*. 2013;110(45). doi:10.1073/pnas.1308253110
66. Langguth P, Bohner V, Heizmann J, et al. The challenge of proteolytic enzymes in intestinal peptide delivery. *J Control Release*. 1997;46(1–2):39–57. doi:10.1016/S0168-3659(96)01586-6
67. Hayhoe RPG, Kamal AM, Solito E, Flower RJ, Cooper D, Perretti M. Annexin 1 and its bioactive peptide inhibit neutrophil-endothelium interactions under flow: indication of distinct receptor involvement. *Blood*. 2006;107(5):2123–2130. doi:10.1182/blood-2005-08-3099
68. Lim LHK, Pervaiz S. Annexin 1: the new face of an old molecule. *FASEB J*. 2007;21(4):968–975. doi:10.1096/fj.06-7464rev
69. Girol AP, Mimura KKO, Drewes CC, et al. Anti-inflammatory mechanisms of the annexin A1 protein and its mimetic peptide Ac2-26 in models of ocular inflammation in vivo and in vitro. *J Immunol*. 2013;190(11). doi:10.4049/jimmunol.1202030
70. Walther A, Riehemann K, Gerke V. A novel ligand of the formyl peptide receptor. *Mol Cell*. 2000;5(5):831–840. doi:10.1016/S1097-2765(00)80323-8
71. Maderna P, Yona S, Perretti M, Godson C. Modulation of phagocytosis of apoptotic neutrophils by supernatant from dexamethasone-treated macrophages and annexin-derived peptide Ac2–26. *J Immunol*. 2005;174(6):3727–3733. doi:10.4049/jimmunol.174.6.3727
72. Sugimoto MA, Vago JP, Teixeira MM, Sousa LP. Annexin A1 and the resolution of inflammation: modulation of neutrophil recruitment, apoptosis, and clearance. *J Immunol Res*. 2016;2016. doi:10.1155/2016/8239258
73. Cristante E, McArthur S, Mauro C, et al. Identification of an essential endogenous regulator of blood–brain barrier integrity, and its pathological and therapeutic implications. *Proc Natl Acad Sci*. 2013;110(3):832–841. doi:10.1073/pnas.1209362110
74. Park J-C, Baik SH, Han S-H, et al. Annexin A1 restores $A\beta_{1-42}$ -induced blood-brain barrier disruption through the inhibition of RhoA-ROCK signaling pathway. *Aging Cell*. 2017;16(1):149–161. doi:10.1111/acel.12530
75. Lacerda JZ, Drewes CC, Mimura KKO, et al. Annexin A12–26 treatment improves skin heterologous transplantation by modulating inflammation and angiogenesis processes. *Front Pharmacol*. 2018:9. doi:10.3389/fphar.2018.01015
76. Hebeda CB, Sandri S, Benis CM, et al. Annexin A1/Formyl peptide receptor pathway controls uterine receptivity to the blastocyst. *Cells*. 2020;9(5). doi:10.3390/cells9051188
77. Sheikh MH, Errede M, d'Amati A, et al. Impact of metabolic disorders on the structural, functional, and immunological integrity of the blood-brain barrier: therapeutic avenues. *FASEB J*. 2022;36(1). doi:10.1096/fj.202101297R
78. Lyngstadaas AV, Olsen MV, Bair JA, et al. Pro-resolving mediator annexin a1 regulates intracellular Ca2+ and mucin secretion in cultured goblet cells suggesting a new use in inflammatory conjunctival diseases. *Front Immunol*. 2021:12. doi:10.3389/fimmu.2021.618653